Climatic Change (2025) 178:97
https://doi.org/10.1007/s10584-025-03937-0

Updated insights on climate change-driven temperature variability across historical and future periods

M.O. Molina[1] · PMM. Soares[1] · MM. Lima[1] · T. H. Gaspar[1] · DCA. Lima[1] · A. M. Ramos[2] · A. Russo[1,3] · R. M. Trigo[1]

Received: 21 March 2024 / Accepted: 21 April 2025 / Published online: 30 April 2025

Abstract
This study highlights the benefits of using high-resolution reanalysis and climate models to assess climate change over time at the subcontinental scale for both present and future periods. The emergence of climate change over the internal variability for each AR6 region is studied by evaluating the decadal frequency distributions of the monthly normalized 2 m temperature anomalies for the 1951-2020 historical and 2015-2100 future periods. To achieve this, monthly averaged daily temperature data from ERA5 and an ensemble of 22 CMIP6 GCMs, following a range of future climate scenarios (SSP1-2.6, SSP2-4.5, SSP3-7.0, and SSP5-8.5), are used. The ERA5 results show a decadal shift in the mean temperature anomalies between 0.6-2.6σ in DJF and 1.1-2.6σ in JJA during the 1951-1980 period. The CMIP6 GCM ensemble can reproduce this historical warming on a climatological timescale, with a large agreement for all regions. Moreover, climate projections strongly suggest that this warming will continue under all climate change scenarios and will be more pronounced by the end of the century. The two most likely scenarios (SSP2-4.5 and SSP3-7.0) show significant evidence that extremely hot temperatures (anomalies of more than three standard deviations (3σ) warmer than the climatology of the 1951-1980 base period) will become the normal climate in Africa and South America for the 2071-2100 period. It is seen that the regional mean temperature anomalies will increase in weak, moderate, and strong forcing scenarios, reaching climatic extremes with expected major implications for the water cycle, agriculture, ecosystems, society, and human health.

Keywords Temperature · Climate anomalies · Climate change · CMIP6 · ERA5

✉ M.O. Molina
mosanchez@ciencias.ulisboa.pt

[1] IDL - Instituto Dom Luiz, Faculdade de Ciências, Universidade de Lisboa, Lisboa 1749-016, Portugal

[2] Institute of Meteorology and Climate Research Troposphere Research (IMKTRO), Karlsruhe Institute of Technology, Karlsruhe, Germany

[3] CEF - Forest Research Centre, Associate Laboratory TERRA, School of Agriculture, University of Lisbon, Lisbon, Portugal

1 Introduction

According to the Sixth Assessment Report of the Intergovernmental Panel on Climate Change (IPCC), global surface temperatures have risen faster since 1970 than in any other 50-year period in the past 2000 years (Zhongming et al. 2022). One of the main consequences of a warmer climate is the occurrence of more (less) frequent and intense extreme heat (cold) events in recent decades (Rummukainen 2012; on Climate Change (IPCC) 2023). Due to anthropogenic global warming (Almazroui et al. 2021a; Molina et al. 2020; Zhongming et al. 2022; Fischer and Knutti 2015), these events are projected to become more frequent and/or intense in the near future (Carvalho et al. 2021), increasing the severity of impacts on natural and human systems (Seneviratne et al. 2012; Díaz et al. 2019; Rohat et al. 2018). Since surface warming is not uniform across regions and seasons and affects different sectors (Bokhorst et al. 2009; Kreyling 2010), addressing the impacts of climate change requires examining the current and future climate evolution on a regional scale.

Historical temperature trends are commonly studied using observational datasets or reanalysis (Donat et al. 2016; Simmons et al. 2017). Previous works have shown the ability of the latest European Center for Medium-Range Weather Forecasts (ECMWF, https://www.ecmwf.int/) reanalysis product, ERA5 (Hersbach et al. 2019, 2020), to adequately reproduce the spatio-temporal characteristics of daily mean temperatures, more accurately in recent decades (Gleixner et al. 2020; Zhu et al. 2021; Collazo et al. 2022; Velikou et al. 2022; Roffe and van der Walt 2023; Yilmaz 2023; Liu et al. 2024; Soci et al. 2024). Most of the shortcomings are due either to the lack of weather station records in the past, which affects the model estimates over time (Yilmaz 2023), or to altitude differences when comparing ERA5 grid points with observations in areas with sharp orography or complex terrain (Wang et al. 2019; Molina et al. 2021; Velikou et al. 2022; Gutiérrez et al. 2024). From a seasonal perspective, ERA5 tends to underestimate summer temperatures and overestimate winter temperatures (Ortega et al. 2021; Choudhury et al. 2023; Yilmaz 2023), resulting in a smaller number of identified heatwaves and a larger number of coldwaves (Roffe and van der Walt 2023).

To investigate plausible future climates, one must rely on climate models. The Coupled Model Intercomparison Project (CMIP, https://www.wcrp-climate.org/wgcm-cmip) is devoted to providing standardized global climate models (GCMs) (Meehl et al. 2000), that are used to produce simulations under different constraints and climate change conditions. In this sense, the Shared Socioeconomic Pathway (SSP) scenarios are driven by different socioeconomic assumptions, ranging from ambitious mitigation to continued emissions growth (Zhongming et al. 2022). The latest CMIP Phase 6 (CMIP6) simulations feature higher spatial resolution and improved parameterization schemes compared to previous versions, resulting in a better representation of the physical and biogeochemical processes of the climate system (Eyring et al. 2016). Previous studies state that the CMIP6 ensemble provides a good or satisfactory representation of spatial variability and the annual temperature cycle (Fan et al. 2020; Lovino et al. 2021; Bazzanela et al. 2023).

Compared to its predecessor CMIP5, CMIP6 shows greater agreement with observations in representing climate variability (Chen et al. 2020; Nie et al. 2020; Voldoire et al. 2019). Although there is a close similarity between the two ensembles in the regional climate sensitivity to climate extremes (Seneviratne and Hauser 2020), the CMIP6 models are significantly warmer than the CMIP5 models at the same level of forcing, and show reduced

internal temperature variability (Almazroui et al. 2020a, b; Sobie et al. 2021). This discrepancy is attributed to the higher climate sensitivity and stronger positive cloud feedback (Zelinka et al. 2020; Tebaldi et al. 2021). Thus, CMIP6 models, which are more sensitive to greenhouse gas emissions, may also have higher variability in temperature on timescales of several decades (Nijsse et al. 2019). Such biases can undermine the accurate assessment of the climate change signal (Maraun 2016). Therefore, it is necessary to assess how well models represent climate variability to interpret their results.

This study aims to update previous research on the signal of climate change on a regional scale, combining an update of the climatology of Hansen et al. (2012) and Hansen and Sato (2016) and extending it into the future, to highlight the increasing importance of extreme events in the evolution of climate change. Earlier work revealed the emergence of a new category of 'extremely hot' summers (Hansen et al. 2012), characterized by temperatures exceeding the reference period mean by three standard deviations. Subsequent research confirmed that recent summer warming in arid and semi-arid subtropical regions has reached at least two standard deviations, far exceeding natural variability (Hansen and Sato 2016).

As the climate is changing and CMIP6 data have become available, the purpose of this study is to extend these findings and take advantage of the benefits or 'added value' of using higher-resolution datasets, such as ERA5. Our first objective is to update the analysis of the decadal warming signal to provide a more detailed and accurate picture of past climate evolution. This is achieved by using the latest high-resolution reanalysis data from ECMWF's ERA5 (Hersbach et al. 2019, 2020), one used by Hansen et al. (2012), from 1951 to 2020. The base period of 1951-1980 was chosen because it represents a period of relatively stable global temperatures before the recent rapid warming, a Holocene climate to which nature and human civilization are well adapted (Hansen et al. 2012), and because it is best to use the longest possible time frame for a decadal assessment of climate change and variability. The second objective is to contextualize these findings within the broader framework of state-of-the-art climate models by examining future climate projections using CMIP6-GCMs under four different SSP scenarios (SSP1-2.6, SSP2-4.5, SSP3-7.0 and SSP5-8.5). The focus is set on the shift in seasonal (December-January-February and June-July-August) mean temperature anomalies and the projected increase in extremely hot events at the regional scale.

The paper is structured as follows: the data and methodology employed are presented in Section 2. Section 3 describes the results, focusing on decadal changes in monthly temperature anomalies and extremely hot events in each region. Firstly, the decadal temperature anomaly distribution for the DJF and JJA seasons is analysed using ERA5 reanalysis data for 1951-2020. Secondly, the historical simulations from CMIP6 (1951-2014) are evaluated, focusing on the ability of the model to represent the present climate anomaly temperature. Finally, the future evolution of the temperature anomaly is examined for the different SSP scenarios and periods. Section 4 discusses the results and the added value of using higher-resolution global climate models and reanalyses to represent regional-scale temperature variability. The main conclusions of the results are summarized in Section 5.

2 Data and methods

2.1 Reanalysis data: ERA5

ERA5 (Hersbach et al. 2018), is the fifth-generation reanalysis developed at the ECMWF. It represents a significant advance in global climate reanalysis, providing hourly estimates for a wide range of atmospheric, oceanic, and land surface variables. The atmospheric component is interpolated to 37 pressure levels from the surface up to 1 Pa, allowing detailed vertical analysis. In addition, ERA5 features a high horizontal grid resolution of 0.25 degrees, which improves its spatial representation and facilitates regional studies. Currently, ERA5 is freely available through the EU-funded Copernicus Climate Change Service (C3S, https://climate.copernicus.eu/) from 1950 to the present. For the analysis of current climate variability, ERA5 monthly means derived from daily surface air temperature data are used for the period 1951-2020, with the years 1951-1980 as a reference. More information on ERA5 characteristics can be found in Hersbach et al. (2019).

2.2 CMIP6 global climate models

Monthly averaged daily temperature data from the Coupled Model Intercomparison Project Phase 6 (CMIP6) GCMs ensemble (available) were obtained from the Earth System Grid Federation (ESGF, https://esgf-node.llnl.gov/search/cmip6). One model representative of each participating institution with available data for the historical (1951-2014), and four future SSP scenarios experiments, such as a low forcing scenario SSP1-2.6 (Sustainability), a medium forcing scenario SSP2-4.5 (Middle of the Road - medium challenges to mitigation and adaptation), an unmitigated forcing scenario SSP3-7.0 (Regional rivalry - high challenges to mitigation and adaptation) and a strong forcing scenario SSP5-8.5 (Fossil-fuelled development - high challenges to mitigation and low challenges to adaptation) (O'Neill et al. 2016), spanning the period 2015-2100 (see Table 1). One member per model is used to reduce the amount of data to be managed while evaluating all models. Each GCM can have a different horizontal resolution, from $0.9^{o} \times 0.9^{o}$ to $2.8^{\circ} \times 2.8$. Thus, to produce spatial analyses, all ERA5 and CMIP6 data were regridded to a common $1.25 \times 1.25^{\circ}$ lat/lon regular grid using conservative remapping before analysis (Schulzweida et al. 2019). An adiabatic temperature correction was applied as in Soares et al. (2012) and Careto et al. (2022) to ensure that all comparisons were calculated at the same height, that is, before the model interpolation, the temperatures were adjusted to sea level with a constant lapse rate of $6.5\ ^{\circ}$ C / km and then corrected again to the orography of the target grid assuming the same lapse rate (Taylor 2024).

2.3 Methodology

The spatiotemporal variability of the seasonal climate at the regional scale is studied by analysing the decadal frequency distributions of monthly surface air temperature for historical (1951-2020) and future (2015-2100) periods. We used the IPCC WGI reference land regions (Iturbide et al. 2020), which is the relevant spatial scale for impact and adaptation studies. To separate between ocean/land regions, cells on the land/sea boundary are assigned

Table 1 CMIP6 Global Climate Models used in the present study

Model name	Institute	Resolution	Reference
ACCESS-CM2	CSIRO-ARCCSS	1.9° × 1.3°	Bi et al. (2013)
ACCESS-ESM1-5	CSIRO	1.9° × 1.3°	Ziehn et al. (2020)
AWI-CM-1-1-MR	AWI	0.9° × 0.9°	Semmler et al. (2020)
BCC-CSM2-MR	BCC	1.1° × 1.1°	Wu et al. (2021)
CanESM2	CCCma	2.8° × 2.8°	Swart et al. (2019)
CAMS-CSM1-0	CAMS	1.1° × 1.1°	Rong (2023)
CESM2	NCAR	1.3° × 0.9°	Danabasoglu et al. (2020)
CMCC-CM2-SR5	CMCC	0.9° × 1.25°	Cherchi et al. (2019)
CNRM-ESM2-1	CNRM-CERFACS	1.4° × 1.4°	Voldoire et al. (2019)
EC-Earth3	EC-Earth-Consortium	0.7° × 0.7°	Consortium et al. (2019)
EC-Earth3-Veg	EC-Earth-Consortium	0.7° × 0.7°	Consortium et al. (2019)
FGOALS-g3	CAS	2° × 2.3°	Li et al. (2020)
GFDL-ESM4	NOAA-GFDL	1.3° × 1°	Dunne et al. (2020)
INM-CM5-0	INM	2° × 1.5°	Volodin et al. (2018)
IPSL-CM6A-LR	IPSL	2.5° × 1.3°	Boucher et al. (2020)
KACE-1-0-G	NIMS-KMA	1.9º × 1.3º	Lee et al. (2020)
MIROC6	MIROC	1.4° × 1.4°	Tatebe et al. (2019)
MPI-ESM1-2-HR3	MPI-M	0.9° × 0.9°	Gutjahr et al. (2019)
MRI-ESM2-0	MRI	1.1° × 1.1°	Yukimoto et al. (2019)
NorESM2-MM	NCC	2.5° × 1.9°	Seland et al. (2020)
TaiESM1	AS-RCEC	0.9º × 0.9º	Wang et al. (2021)
UKESM1-0-LL	MOHC	1.9° × 1.3°	Sellar et al. (2019)

to a specific region according to their reference point. This means that if the centre of a cell falls on the sea, it is classified as maritime, even if part of the cell is on land (or vice versa).

Following the approach suggested by Hansen et al. (2012), the shift of seasonal mean temperature in standard deviation units is presented, highlighting the anomalous signal-to-noise ratio of seasonal extremes. For each decade or period analysed, the seasonal anomalies in SD units are calculated for each grid point. Density curves are then constructed for each region using these values. This methodology is useful for identifying locations where the warming signal arises outside the internal variability of the region.

The distribution of temperature anomalies follows a normal distribution (Gaussian or bell curve), where the standard deviation (σ) defines how far the normal distribution is spread around the mean. In a normal distribution, 95% of all values fall within the range of mean-2σ, mean+2σ, and 99.7% fall between the range of mean-3σ, mean+3σ, so if a single value falls outside 3σ, it is considered an extreme anomaly. Decadal anomalies are computed over the 1951-1980 climatology, as in Hansen et al. (2012) and Hansen and Sato (2016).

First, the distribution of temperature anomalies (in standard deviation units) is presented for each grid point of the ERA5 reanalysis data for the boreal winter (December-January-February, DJF) and the boreal summer (June-July-August, JJA) for the contemporary period 1951-2020, updating and extending the studies by Hansen et al. (2012) and Hansen and Sato (2016), thus providing a more recent perspective on seasonal climate variability. Second, seasonal anomalies are computed for two 30-year contemporary periods (1951-1980 and 1985-2014) to compare the performance of CMIP6 GCMs in a historical context with ERA5 for each region (Zhongming et al. 2022). The reason for selecting 30-year anomalies

instead of decadal anomalies is to reduce the internal variability among GCMs (Jain et al. 2023), since GCMs are effective in simulating large-scale global circulation patterns. At the same time, they exhibit challenges in accurately capturing decadal and local variability. The future climate change signal is then analysed for the near (2015-2040), middle (2041-2070) and long-term (2071-2100) periods, considering four different SSP scenarios (SSP1-2.6, SSP2-4.5, SSP3-7.0 and SSP5-8.5), with the CMIP6 GCMs. These periods are widely used in climate projections, including in IPCC assessments, to represent near-, mid-, and long-term futures (Zhongming et al. 2022).

Changes in the decadal distribution of temperature anomalies can be assessed visually, but also through the μ parameter, which represents the scale parameter of the corresponding normal distribution. The 'shift' of the bell curve for each decade analysed relative to the base period, is calculated by finding the μ yielding the best least-mean-square fit of the data to the common representation of the probability density function of the corresponding normal distribution:

$$f(x) = \frac{\exp\left(-\frac{(x-\mu)^2}{2\sigma^2}\right)}{\sigma\sqrt{2\pi}} \tag{1}$$

Thus, the 'shift' metric represents the difference between the seasonal mean temperature during a decade and the climatological (1951-1980) in standard deviation units. This reflects the extent to which regional climate variability has changed and the impact of climate change mitigation measures.

3 Results

3.1 Changes in present climate with ERA5

The distribution of decadal temperature anomalies (in standard deviation units) between 1951 and 2020 for DJF (first column) and JJA (second column) is shown in Fig. 1 for different reference regions. The supplementary material contains results for all regions. Here, a representative subset of regions is presented, considering those that exhibit greater disparities in regional warming or distinct characteristics in the shape of their anomaly distribution curves. For each region, the shift of the approximate bell curve for each decade relative to the base period (1951-1980) and the percentage of events above 3σ are analysed.

Overall, the results show a clear shift in the distribution of temperature anomalies towards positive values, larger over time in all regions, more pronounced in the last two decades, and larger in their respective summers than in winter. In the Northern Hemisphere regions (N. Central America, Mediterranean, Arabian Peninsula and Western Africa), the shift of the bell curve in 2011-2020 relative to the 1951-1980 baseline is of 0.6-1.1 standard deviations (σ) during the boreal winter (DJF) and 1.1-2.5σ during the boreal summer (JJA), indicating a more pronounced warming in summer compared to winter. In the last decade (2011-2020), the South American Monsoon and S.E. Asia regions show a shift of 1.5-2.6σ in DJF and 0.6-2.6σ in JJA, respectively. In E. Antarctica during the summer months (DJF), the decadal distributions deviate from a typical bell curve and exhibit a bimodal pattern. It displays a

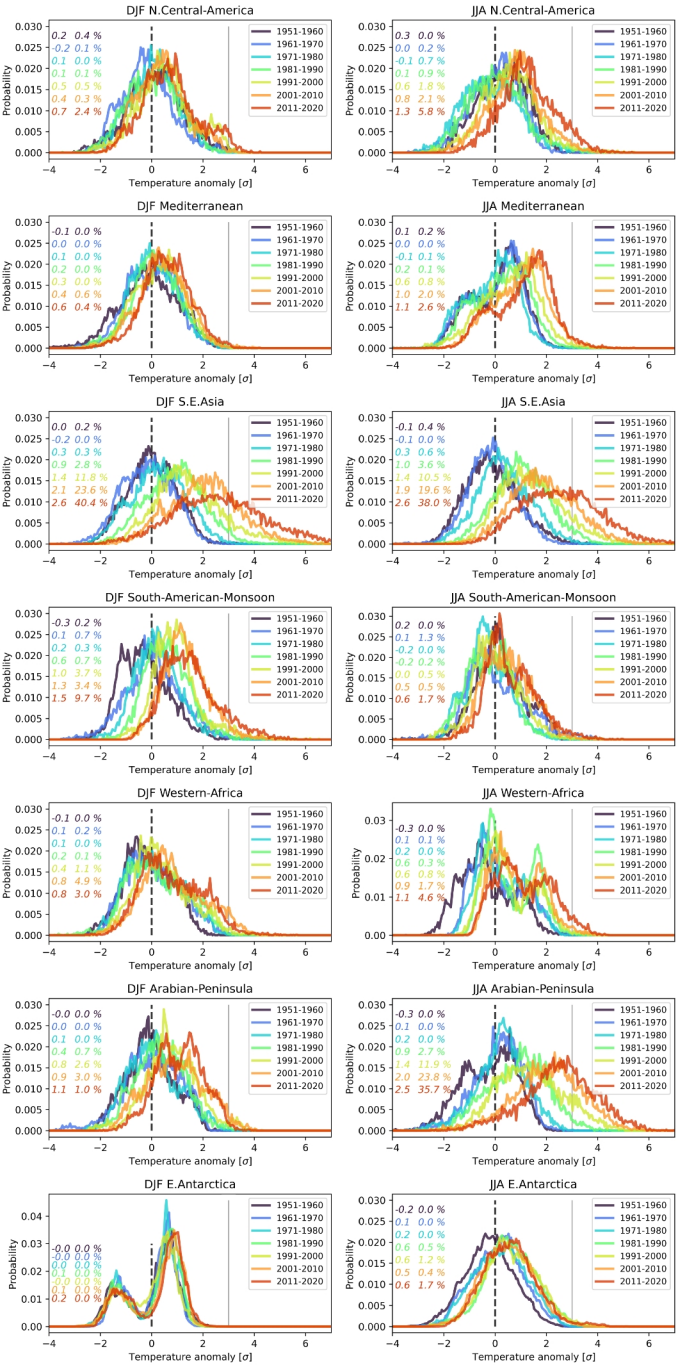

Fig. 1 Frequency of occurrence of DJF (left column) and JJA (right column) local temperature anomalies (relative to 1951-1980 mean) divided by local standard deviation, obtained by counting grid boxes with anomalies in each 0.05 interval. The area under each curve is unitary. The decadal shift is shown in the left column and the percentage of events above 3σ in the right column

minimum in the centre of the distribution, with one peak occurring around -1.5σ on the left and a higher peak around +1σ on the right. This means that temperatures behave differently in two dominant situations. Looking at the mean Antarctic DJF temperature shift, no trend is detected until 2000, after which a warming trend emerges and continues to the present. This late warming is consistent with a shift in the Southern Annular Mode (SAM) towards its positive phase, which influences the Antarctic temperature mainly in summer, warming the Antarctic Peninsula and cooling East Antarctica (Goosse et al. 2012; Turner et al. 2020, 2021; Saurral and Raggio 2023). The magnitude of warming is more pronounced during the boreal summer (JJA), with an increase of 0.6σ, compared to 0.2σ in DJF.

As previously shown by Hansen et al. (2012) for the 1981-2010 period on a global scale, the distributions normalized anomalies for the last decades become less peaked than the normal distribution, more visible in the regions of Asia, South America, Arabian Peninsula and Africa, due to greater temperature variability during the last two decades. In recent decades, a flattening of the curves has been observed for regions in Africa, Asia and South America during summer (Fig. 1) due to a decrease in mean temperatures accompanied by an increase in the frequency of extreme monthly heat events. Interestingly, in the Mediterranean and Western Africa, instead of a flattened curve, two maxima have been observed in JJA, due to a greater increase in the events around 2σ.

Hansen et al. (2012) found that the frequency of extreme temperature anomalies (>3σ) in the period 2006-2011 covered 4% to 13% of the global land surface, while there were no such events during the 1951-1980 period. Here, it is seen that the frequency of those events in DJF (first column of Fig. 1) in the last decade corresponds to 2.4% in N. Central America, 0.4% in the Mediterranean, 3% in Western Africa, and 9.7% in South-American-Monsoon. In S.E. Asia, the anomalies above 3σ in DJF (boreal winter) quadrupled in the last two decades, from 11.81% in the nineties to 40.42%. In JJA (second column of Fig. 1), the increase of extreme events that occurred in the 2011-2020 period is particularly striking for some regions, reaching 38% in S.E. Asia and 35% in the Arabian Peninsula, these values being much higher than those observed in the previous decade (19.6% and 23.8%, respectively). In the remaining regions, the increase in extreme heat anomalies is also more pronounced from the 2010s onwards.

Figure 2 illustrates the spatial distribution of seasonal climate change signals during recent decades. As expected, there is an increase in the proportion of land area experiencing temperature anomalies above a certain threshold. In boreal winter, anomalies greater than 2σ are obtained for the 2011-2020 decade in Africa, South America and South East Asia. On a global scale, the percentage of the area above 3σ increased from 0.4% in the decade 2001-2010 to 1.1% in DJF and from 0.4 to 1.2% in JJA during 2011-2020 over the polar region of Canada, similar to Hansen and Sato (2016). In the last decade, extremely hot summer events have occurred for the first time in Greenland, and events above 4σ and 5σ increased, covering 0.3% and 0.1% of the global land area, respectively. Global warming is more intense in the intertropical zone for both seasons. As expected in Europe (Vautard et al. 2023), larger anomalies are observed over the Mediterranean region, reaching 1.5σ in the boreal summer. This value is exceeded in Central America, parts of the Mediterranean Africa, the Arabian Peninsula, and South East Asia. Lower values are observed for the DJF months, when the warming is about 0.25-0.5σ over most of North America, Europe, Asia, North Africa, and Oceania.

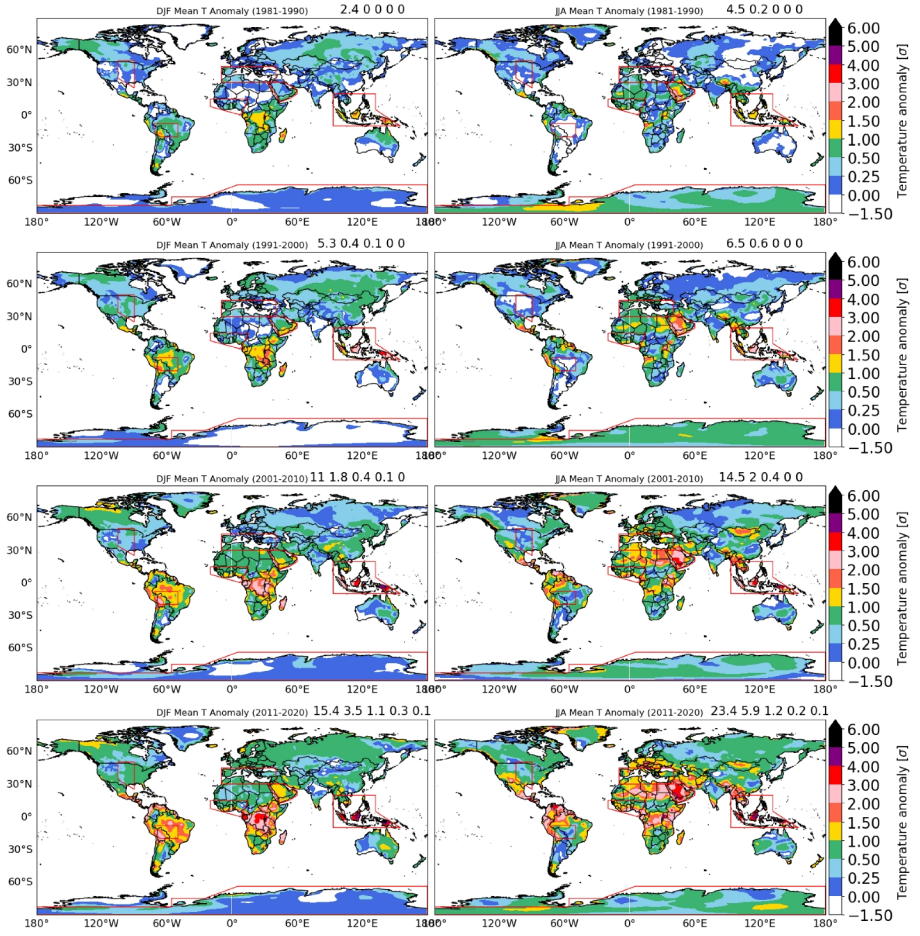

Fig. 2 Frequency of DJF (left) and JJA (right) temperature mean anomalies at each ERA5 grid point (relative to 1951-1980 mean) divided by the local standard deviation in the (**a**) 1981-1990, (**b**) 1991-2000, (**c**) 2001-2010 and (**d**) 2011-2020 decades. The numbers on each map refer to the cumulative percentage of the area covered by anomalies greater than 1,2, 3, 4 and 5 standard deviations

3.2 Evaluation of CMIP6 model performance

To assess the ability of current state-of-the-art GCMs to reproduce historical temperature distributions, the changes in temperature anomalies were computed for the climatic periods 1951-1980 and 1985-2014, taking the former as a reference. This analysis was performed using the CMIP6 GCM ensemble and compared against the ERA5 reanalysis dataset, as shown in Fig. 3. In general, CMIP6 models are able to reproduce temperature anomalies on a climatological scale and the larger warming in boreal summer than in winter described by ERA5. Comparing the climate change signal between ERA5 and the CMIP6 ensemble mean in Fig. 3, it is seen that the bell curve shift is overall well represented in all regions. Results show a maximum underestimation of the bell curve shift of 0.8σ in S.E. Asia, 0.4σ in Western Africa during DJF, and 0.8σ in the Arabian Peninsula during JJA. This underes-

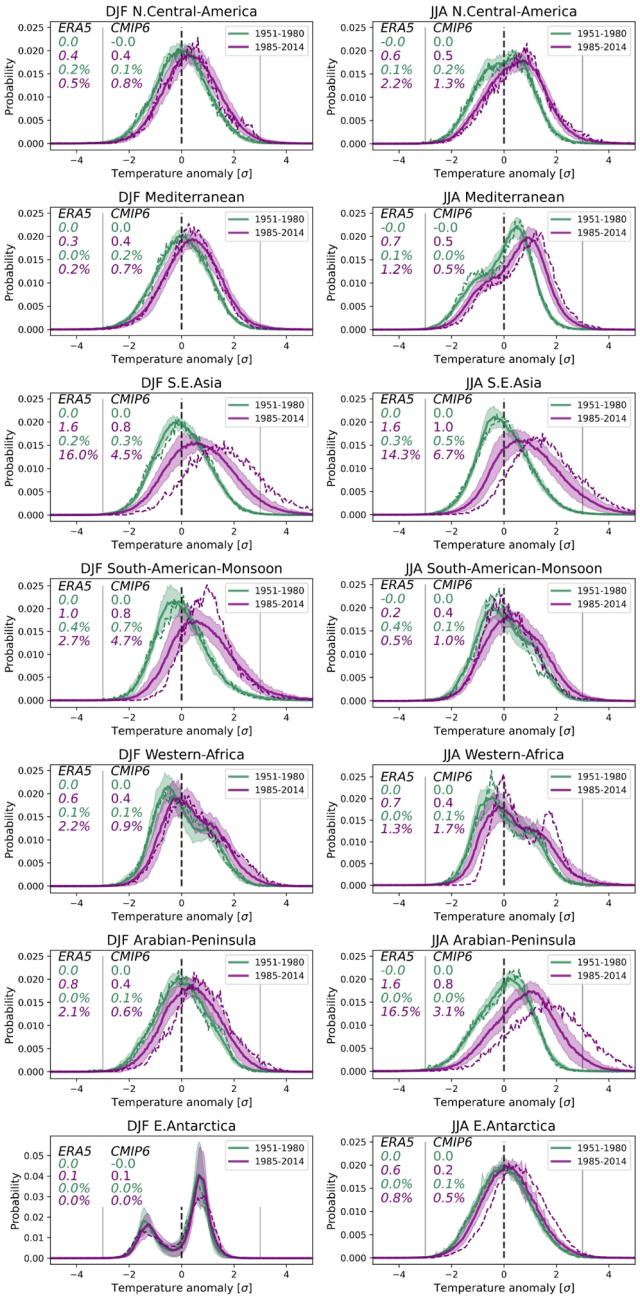

Fig. 3 Frequency of occurrence of DJF (left column) and JJA (right column) local temperature anomalies for the climate periods 1951-1980 (green) and 1985-2014 (purple) (relative to the 1951-1980 mean) divided by local standard deviation, obtained by counting grid boxes with anomalies in each 0.05 interval. The CMIP6 GCMs are represented by the solid line and the ERA5 data by the dashed line. The shaded area represents the mean plus/minus the standard deviation (CMIP6 model variability) for each period. The 30-year period shift and the percentage of events above 3σ are shown on the upper left of the panels

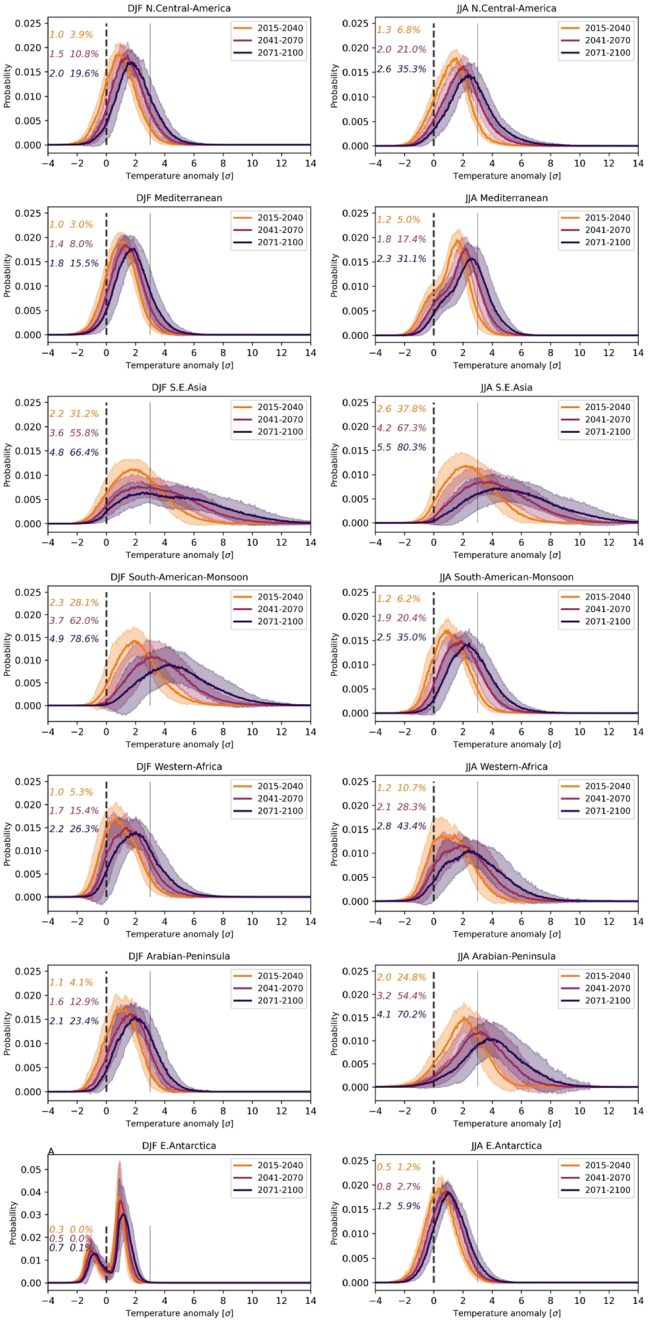

Fig. 4 Frequency of occurrence of DJF local temperature anomalies in the SSP2-4.5 (relative to the 1951-1980 mean) divided by local standard deviation, obtained by counting grid boxes with anomalies in each 0.05 interval. The area under each curve is unitary. The shift is shown in colours on the left of the curve and the percentage of events above 3σ on the right. The map represents the 2071-2100 seasonal mean anomaly of each grid point in reference to the 1951-1980 period

timation of the signal-to-noise ratio of temperature anomalies could affect the representation of future global warming by models.

The models demonstrate limitations in accurately representing extremes, with some underestimation in the frequency of hot events while overestimating cold events. During DJF (as shown in the first column of Fig. 3), extreme values are substantially underestimated, by 11.4% over Southeast Asia and 13% over the Arabian Peninsula, with comparable discrepancies observed across regions of other continents. In JJA (second column of Fig. 3), GCMs tend to underestimate extremes over Asia, the Mediterranean, and the Arabian Peninsula, and overestimate them in Western Africa and South American Monsoon (boreal winter), with similar values to ERA5 in the other regions.

3.3 CMIP6 climate projections

The climatic evolution of temperature variability is analysed for four SSP scenarios (SSP1-2.6, SSP2-4.5, SSP3-7.0 and SSP5-8.5) for three different periods: near (2015-2040), middle (2041-2070) and long-term (2071-2100). Overall, the temperature anomaly curves exhibit a shift and flattening to the right, indicating both an increase in mean temperatures and an increase in the frequency of monthly extreme heat events over the 21st century. The magnitude of these changes is expected to intensify with increasing radiative forcing (SSP scenario) and with time (Lehner et al. 2020), as shown in Figs. 5, 7 and Supplementary Figures S3-S11. Within this framework, by the 2071-2100 period, the bell curve shift during DJF (JJA) is projected to exceed 1.2 (1.6)σ across all regions except Antarctica, where the warming is smaller (0.7 (1.2)σ Figure S5). The larger climate change signal is seen in the equatorial regions of S.E. Asia, the Arabian Peninsula, Western Africa and the South American Monsoon, reaching a shift of 4.8 (5.5), 2.1 (4.1), 2.1 (4.1) and 4.9 (2.5)σ in DJF (JJA), respectively.

In a moderate scenario (SSP2-4.5), the percentage of anomalies above 3σ is likely to remain below 20 (36)% in boreal winter (boreal summer) for N. Central America and the Mediterranean by the end of the century. Instead, extremes for the Arabian Peninsula, South American Monsoon and S.E. Asia regions could reach 70-80% in their respective summers by the end of the century. In E. Antarctica, the warming would be 0.5σ greater in JJA than in DJF, with a shift that could reach 1.2σ by the end of the century.

Looking at the spatial distribution of anomalies larger than 3σ in the SSP2-4.5 scenario (pink colour in Fig. 5), they are mainly located mainly in S.E. Asia in 2015-2040, covering 0.3% of the global land area, and would extend over the Arabian Peninsula, Western Africa and Central America in 2041-2070, covering 1.8% of the area. In 2071-2100, the so-called 'hot-summers' would reach 4 (5.4)% in DJF (JJA), and the events above 5σ would appear in South East Asia, covering 0.3% of the area.

Although regional warming under the SSP3-7.0 scenario is projected to be similar to the moderate SSP2-4.5 scenario in the near future, it is expected to diverge as we move to the 2071-2100 period (Fig. 6). The summer shows the highest probability of values above 3σ, especially in S.E. Asia (90%) and the Arabian Peninsula (83%) during JJA, and S. American Monsoon (90%) during DJF.

Figure 7 displays the spatial distribution of seasonal normalized temperature anomalies for the SSP3-7.0 scenario. The distribution of the highest anomalies is quite similar to the SSP2-4.5 scenario (Fig. 5), particularly for the near future period 2015-2040. The differ-

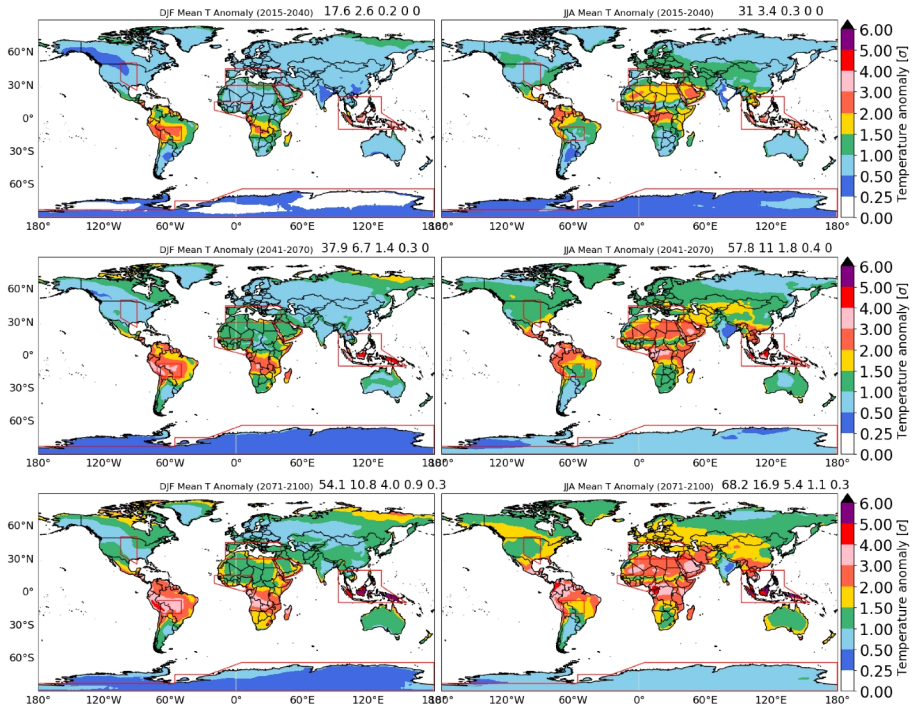

Fig. 5 Frequency of DJF (left) and JJA (right) temperature mean anomalies of each CMIP6 ensemble mean grid point (relative to 1951-1980 mean) divided by the local standard deviation in the (**a**) 2015-2040, (**b**) 2041-2070, and (**c**) 2071-2100 decades, for the SSP2-4.5 scenario. The numbers on each map are the cumulative percentage of the area covered by anomalies greater than 1,2, 3, 4 and 5 standard deviations

ences become more pronounced at the end of the century, especially in high-latitude regions for DJF and over Africa and Antarctica for JJA, reaching 10.2% of the global land area.

Looking at the most optimistic scenario (SSP1-2.6, Figures S3 and S4), it is seen that the warming will continue in the near and middle term, and it will stabilize by the end of the century. In 2071-2100, the shift will reach 3.2σ (3.6) in South Asia, 2σ (2.7) in Western Africa, 3.3σ (1.7) in the South American Monsoon, 1.4σ (2.7) in the Arabian Peninsula and about 1.2σ (1.5) in DJF (JJA) in the other regions. Greater warming leads to a higher frequency of extremes. This means that even in a low forcing scenario (SSP1-2.6), the anomalies above 3σ in JJA will reach 8-10% for the Northern Hemisphere regions and 40-50% for South America and Africa, and almost 60% in S.E. Asia. In Antarctica, there will be no major change in the boreal summer (JJA) temperature anomalies. However, summer hot extremes above 3σ could increase by 2% by 2100.

In the high-end forcing scenario (SSP5-8.5, Figures S10 and S11), extreme temperature events that are rare today are projected to become normal in the future in JJA in North America, Northern Europe, South Asia and the Mediterranean, where the shift would be above 3σ (50% of the events above 3σ). In Western Africa and S. American Monsoon regions, the shift would be even larger, with 3.4σ (4.7) and 8.3σ (4.3) in DJF (JJA), and more than 70% of the events above 3σ. In the Arabian Peninsula, the change would be 3.5σ in DJF,

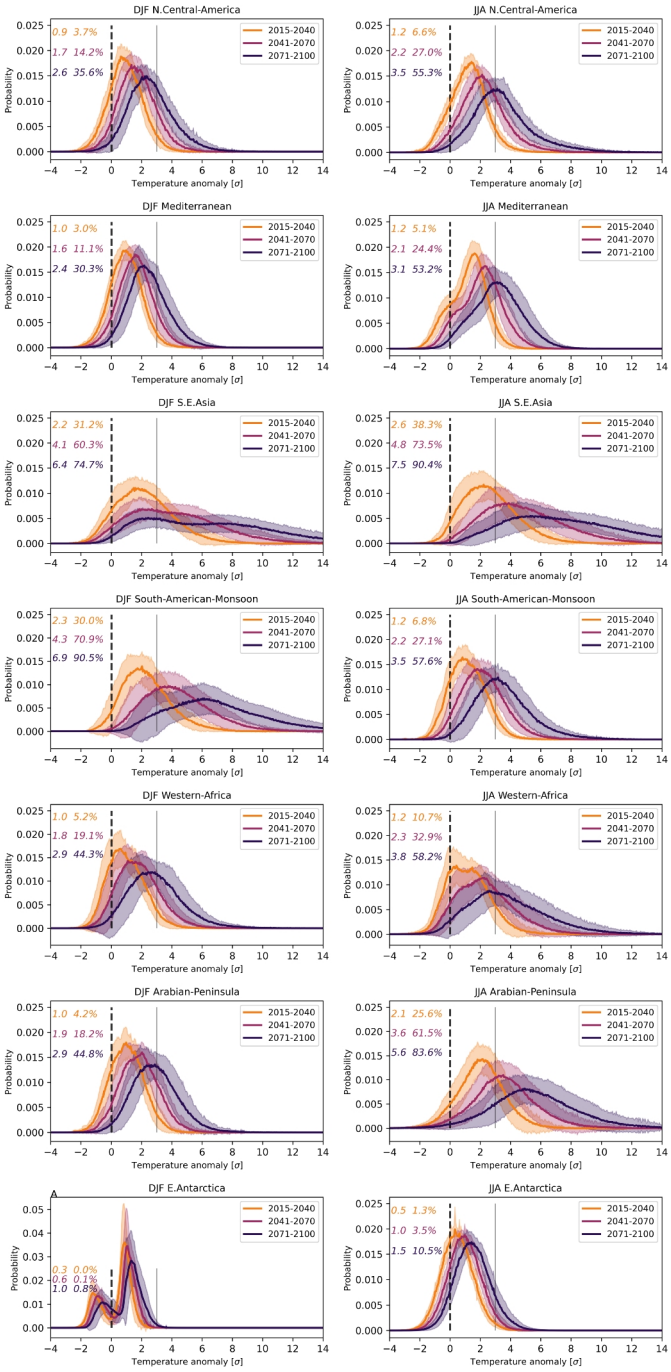

Fig. 6 As Fig. 4, for the SSP3-7.0 scenario

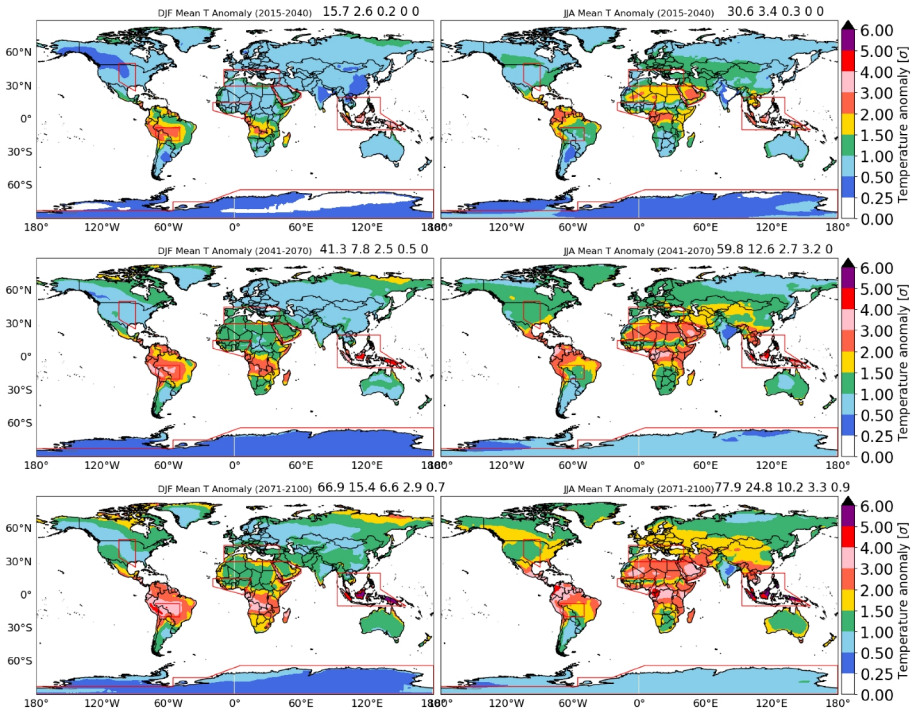

Fig. 7 As Fig. 5, for the SSP3-7.0 scenario

but in JJA this value could double and reach the 88%. Except for Antarctica, all regions will experience a temperature shift upwards of 1.4σ in the middle term and more than 1.9σ at the end of the century, regardless of the season, with S.E. Asia being the most affected region with a change of 9.1σ in JJA. In DJF (Figure S8), the small anomaly values for Europe and the large values for South America stand out. In the Mediterranean region, only 5% of the events will exceed 3σ in the middle-term and 19% in the long-term, while in South America it will surpass 77% of the events if this scenario occurs. In JJA (Figure S9), anomalies above 3σ are projected to exceed 50% across regions in the Northern Hemisphere and Oceania, with values reaching up to 77% in Africa during the period 2071-2100. The spatial pattern of normalized temperature anomalies (Figure S10) shows that the areas with larger shifts will be Central America and the northern part of South America and Africa, especially the Congo and Sahara regions, where the shift could be 5.8σ (4.1) and 4.4σ (4.4) in summer (winter), respectively. These values are smaller than the annual shift observed in Harrington (2021) and larger than the daily mean temperature anomalies obtained from a CMIP5 ensemble for the similar high-end scenario (RCP8.5), probably due to the different drivers of temperature variability at annual, seasonal and daily timescales (Fischer and Schär 2009; Molina et al. 2021).

4 Discussion

The latest IPCC AR6 report (Zhongming et al. 2022) evaluates temperature anomalies on a subcontinental scale, considered the relevant scale for impact assessment and adaptation studies. To achieve this, higher-resolution models and reanalysis data provide information at increasingly finer scales that are more suitable for regional analysis. In addition, employing a multimodel approach is crucial to increase the robustness of the results. A more accurate representation of orography and surface heterogeneities, such as land-sea contrasts, through high-resolution reanalysis, improves and adds value to the representation of the spatiotemporal characteristics of daily mean temperatures (Zhu et al. 2021; Velikou et al. 2022; Yilmaz 2023).

While Hansen et al. (2012) and Hansen and Sato (2016) framed their work in the context of climate change attribution and inequality and the imbalance between the nations that emit the most CO2 and those that suffer the most from climate change, this study does not attempt to address attribution or such inequalities. It is therefore not strictly an update of those studies using new datasets. Instead, it focuses on reporting changes in future temperature projections. The use of a higher resolution reanalysis grid (interpolated to 100 km) compared to the 250 km grid used by Hansen and Sato (2016) allows for a clearer description of the regional climate characteristics, demonstrating the added value of using high-resolution models in regional studies. This is evident in the sharper distribution curves observed in high-latitude regions of North America, Europe and Russia, where the climate change is less pronounced, as well as the two distinct maxima in the curves for the Mediterranean and South Asia, reflecting a rapid increase in the frequency of temperature extremes. A notable case is the bimodal temperature distribution observed in East Antarctica during DJF (in West Antarctica the bell follows a normal shape). Although this pattern is not commonly seen, previous studies have attributed it to an increase in the positive phase of the Southern Annular Mode, which warms the Antarctic Peninsula while cooling East Antarctica during summer (Goosse et al. 2012; Turner et al. 2021; Saurral and Raggio 2023).

Previous studies have shown that the acceleration in the frequency and intensity of extreme events in recent years has been even greater than that of mean temperature (Byrne 2021; Patterson 2023). Our results point to a larger increase in the tail of the temperature distribution anomalies in regions such as the Mediterranean or South Africa. The standard deviation of the local seasonal mean surface temperature over a period of years is a measure of the typical variability of the seasonal mean temperature over that period (Hansen et al. 2012). This method allows us to evaluate the changes in climate variability, i.e., how different it is from historical variability, and to consider whether there is a significant climate change. While an anomaly by itself does not inform on the associated variability to which ecosystems are accustomed, a change in normal variability would necessarily impact the ecosystems living there.

Our results characterize the warming signal over recent periods and project its continuation under different climate change scenarios. This allows us to quantify the reduction in monthly extreme cold events and the increase in hot extremes. The climate change signal is more pronounced during JJA on all continents, except South America. The stronger warming of the Northern Hemisphere regions, where most of the global land surface is located, could be related to greater warming over land regions than over the oceans (Tebaldi et al. 2021). Compared to the findings of Hansen and Sato (2016) for the 2005-2015 period, our

analysis reveals smaller temperature shifts in N. Central America in JJA (0.5-0.8σ here versus 1.1σ there), as well as in China (E. Asia) and the Sahara region. Conversely, the temperature shift in India and South East Asia (S.E. Asia and S.E. Asia) is considerably larger in both seasons, while the results for the other regions are comparable.

The decadal increase in monthly hot extremes is generally more substantial than mean temperatures, likely due to the amplification of temperatures in warmer and drier environments, and an increase in the local meridional temperature gradient. This enhanced gradient facilitates the advection of hotter air masses to higher latitudes, leading to more extreme temperature events (Huntingford et al. 2013; Byrne 2021; Patterson 2023). The increase in events larger than 3σ with global warming may also be associated with regions and periods of high atmospheric pressure systems (Hansen et al. 2012; Suarez-Gutierrez et al. 2020).

To interpret future climate projections accurately, the CMIP6 models must be evaluated by comparing historical simulations with observed or ERA5 data to assess how well CMIP6 models respond to known historical forcing. Model performance varies by region and season (Almazroui et al. 2021b; Dias and Reboita 2021; Cardoso and Soares 2022; Molina et al. 2022; Bazzanela et al. 2023; Molina et al. 2024). While the CMIP6 models demonstrate incremental improvements in the representation of atmosphere and ocean extreme heat events in the Australian region (Grose et al. 2020), they tend to underestimate mean temperatures in central South America in winter (Ortega et al. 2021) and cold extremes at high latitudes (Kim et al. 2020). Comparing with observations, Almazroui et al. (2021b) and Dias and Reboita (2021) found that the ensemble performs well over South America, but overestimates air temperature in the Amazon and north of Argentina. As in Bazzanela et al. (2023), the results presented here confirm that the CMIP6 models perform well over South America in JJA, although they underestimate the mean temperature anomalies of DJF compared to ERA5. If models underestimate the forced response to greenhouse gases in the historical climate, this discrepancy may persist and even be magnified as global warming increases (Vautard et al. 2023).

According to the results, the future increase in climate variability will not be uniform within regions and seasons. Spatial projections for the 2071-2100 period, relative to 1951-1980, indicate that the emergence of climate change is greatest in equatorial regions. This is consistent with the warming and increase of hot extremes projected by prior studies (Almazroui et al. 2021a; Harrington 2021). In the SSP2-45 scenario, the monthly temperature shift would exceed 1.2σ during DJF and 1.6σ during JJA in most regions by 2071-2100, except in Antarctica. By the end of the century, JJA regional climate change signal could reach 2σ in the Sahara, 3σ in Central America and 3.6σ in South East Asia. In regions with smaller temperature increases, events currently considered extreme (>3σ) would become normal events, while this threshold would be significantly exceeded in Southeast Asia, Brazil and the intertropical regions. This is consistent with Almazroui et al. (2021a), which identifies the Amazon, Brazil, the Mediterranean, Southern Africa, and parts of Australia as future hotspots for increasing hot and dry compound events.

In a scenario where no further mitigation measures are implemented beyond current policies (SSP3-7.0), the bell curve shift in DJF would exceed 2σ over Africa, the Mediterranean, Asia, the Arabian Peninsula, and most parts of South America. In addition, the "hot summers" defined by Hansen et al. (2012) as events above 3σ could account for more than 30% of summer days in Northern Hemisphere regions, and more than 60% in South America and Southern Africa. In the worst-case scenario (SSP5-8.5), extreme events, which

are rare today, could become the norm in JJA across North America, Europe, Asia and Oceania (Carvalho et al. 2021). The enhanced warming during JJA can be attributed to the northward shift of the intertropical convergence zone caused by the expansion of the Hadley cell (Schneider et al. 2014; Xian et al. 2021). An exception is observed over India, where the projected variability is greater during winter, as the warming reported by Almazroui et al. (2020a). In contrast, the larger increase in JJA variability in China, compared to DJF, differs from the CMIP5 ensemble projections, which indicate significant warming during autumn/winter and late spring (Tian et al. 2015).

Our results are in line with those reported by Almazroui et al. (2020b, 2021a, 2021b), where robust temperature increases are already detected from SSP1-2.6. In the SSP1-2.6 scenario, climate variability intensifies and extends to encompass more temperate regions in both seasons. Extremes exceeding 2σ are obtained over the high latitudes of Asia and North America. These results are coherent with the greater summer warming projected over the Sahara and Mediterranean regions, and in contrast with the greater warming in Northern Europe in winter than in summer (Almazroui et al. 2020b; Fan et al. 2020; Carvalho et al. 2021). This is due to the larger standard deviation experienced in the reference period (1951-1980) in this area and the Arctic regions (not shown), resulting in a lower future anomaly. Additionally, South East Asia shows the largest anomalies, despite Hamed et al. (2022) reporting a smaller projected temperature increase in CMIP6 compared to CMIP5 for Southern Asia.

Comparing our findings with CMIP5 projections, the overall results are consistent, particularly regarding the pronounced warming in equatorial regions (Harrington 2021). However, the CMIP6 ensemble projects less warming over South East Asia (Hamed et al. 2022) and more warming over Northern Africa and China than the CMIP5 ensemble (Tian et al. 2015).

5 Conclusions

The purpose of this study is twofold: (1) to update the climate change studies carried out by Hansen et al. (2012) and Hansen and Sato (2016) globally at the decadal and subcontinental scales, taking advantage of the latest available reanalysis (ERA5), with a higher spatial resolution, from 1951 to 2020, and (2) to provide a similar methodological assessment when looking into the future with the state-of-the-art global simulations from the CMIP6 project, under four different SSP scenarios. For the climate change analysis, a multimodel ensemble based on 22 GCMs from CMIP6 is examined for three future time slices (2015-2040, 2041-2070 and 2071-2100), under four SSP scenarios ranging from low to a high forcing scenario (SSP1-2.6, SSP2-4.5, SSP3-7.0 and SSP5-8.5). This approach allows for the assessment of changes in climate variability and the detection of significant deviations from the current climate to which local ecosystems have adapted. Changes in typical climate variability are bound to affect these ecosystems. An accurate prediction of future climate conditions is essential for fostering mitigation and developing effective adaptation strategies to address climate change, especially in response to extreme events (Díaz et al. 2019; Rohat et al. 2018).

The results indicate a significant rightward shift in monthly surface temperature anomalies distribution across all regions, especially in the past decade (2011-2020). This confirms

and amplifies the strong warming observed by Hansen et al. (2012) from 2001 to 2010. Besides, the shape of the temperature frequency distribution curve is broadening, with the right tail becoming longer. This evolution is due to generalized higher standard deviation values in most regions coupled with a decrease (increase) of cold (hot) monthly extreme temperatures. The increase in monthly hot extremes is more pronounced in summer than in winter in all continents, with regions belonging to Asia, South America and Africa showing an even greater increment.

Using finer spatial resolution data adds value to the temperature anomalies study at the subcontinental scale. A novelty of these results is the bimodal curves over East Antarctica in DJF and the particularities over West Africa and the Mediterranean regions in JJA.

Overall, the CMIP6 ensemble has been shown to reproduce the ERA5 temperature frequency distributions, the climatological mean temperature shift, and the greater warming in summer than in winter.

Future climate projections show that warming will amplify over time with increasing emissions. In a low forcing scenario (SSP1-2.6), although the warming will continue in the near and mid-century, it will stabilize by the end of the century with a shift of about 1.2σ (1.5) in DJF (JJA) in the Northern Hemisphere regions. This result indicates that taking measures to reduce emissions is paramount in limiting the temperature increases on a regional scale.

It is also important to note that future warming will not be uniform within continents and seasons. The equatorial region would be more affected, extending to higher latitudes in the boreal summer. The climate change signal is greater during JJA than in DJF, due to the greater warming of landmasses relative to the oceans, which are predominantly located in the Northern Hemisphere.

Future studies should prioritize a thorough examination of the regions most vulnerable to the impacts of climate change. The accelerated climate warming observed in recent years could have important implications for human health and ecosystems, particularly in terms of their adaptability in those areas that are already most stressed (Geirinhas et al. 2020).

Supplementary Information The online version contains supplementary material available at https://doi.org/10.1007/s10584-025-03937-0.

Funding Open access funding provided by FCT|FCCN (b-on).
This work was funded by the Portuguese Fundação para a Ciência e a Tecnologia (FCT) I.P./MCTES through national funds (PIDDAC) – UID/50019/2025 and LA/P/0068/2020 (https://doi.org/10.54499/LA/P/0068/2020) M.O. Molina was supported by the Portuguese Fundação para a Ciência e a Tecnologia (FCT) through the DRI/India/0098/2020 project (https://doi.org/10.54499/DRI/India/0098/2020) A.R. acknowledges project DHEFEUS https://doi.org/10.54499/2022.09185.PTDC and UIDB/00239/2020 (https://doi.org/10.54499/UIDB/00239/2020), UIDP/00239/2020 (https://doi.org/10.54499/UIDP/00239/2020), supported by national funds through FCT, and through project references UIDB/00239/2020 (https://doi.org/10.54499/UIDB/00239/2020) and UIDP/00239/2020 (https://doi.org/10.54499/UIDP/00239/2020). DL and AR also acknowledge FCT I.P./MCTES for the FCT through projects https://doi.org/10.54499/2022.03183.CEECIND/CP1715/CT0004 and https://doi.org/10.54499/2022.01167.CEECIND/CP1722/CT0006, respectively. AMR was supported by the Helmholtz "Changing Earth – Sustaining our Future" program. M. M. Lima was supported through the PhD MIT Portugal MPP2030-FCT programme grant PRT/BD/154680/2023.

References

Almazroui M, Saeed S, Saeed F, Islam MN, Ismail M (2020a) Projections of precipitation and temperature over the South Asian countries in CMIP6. Earth Syst Environ 4:297–320

Almazroui M, Saeed F, Saeed S, Nazrul Islam M, Ismail M, Klutse NAB et al (2020b) Projected change in temperature and precipitation over Africa from CMIP6. Earth Syst Environ 4:455–475

Almazroui M, Saeed F, Saeed S, Ismail M, Ehsan MA, Islam MN et al (2021a) Projected changes in climate extremes using CMIP6 simulations over SREX regions. Earth Syst Environ 5(3):481–497

Almazroui M, Ashfaq M, Islam MN, Rashid IU, Kamil S, Abid MA et al (2021b) Assessment of CMIP6 performance and projected temperature and precipitation changes over South America. Earth Syst Dyn 5(2):155–183

Bazzanela AC, Dereczynski C, Luiz-Silva W, Regoto P (2023) Performance of CMIP6 models over South America. Climate Dynamics, pp 1–16

Bi D, Dix M, Marsland S, O'Farrell S, Rashid H, Uotila P et al (2013) The ACCESS coupled model: description, control climate and evaluation. Aust Meteor Oceanographic J 63(1):41–64

Bokhorst SF, Bjerke JW, Tømmervik H, Callaghan TV, Phoenix GK (2009) Winter warming events damage sub-Arctic vegetation: consistent evidence from an experimental manipulation and a natural event. J Ecol 97(6):1408–1415

Boucher O, Servonnat J, Albright AL, Aumont O, Balkanski Y, Bastrikov V et al (2020) Presentation and evaluation of the IPSL-CM6A-LR climate model. J Adv Model Earth Syst 12(7):e2019MS002010

Byrne MP (2021) Amplified warming of extreme temperatures over tropical land. Nat Geosci 14(11):837–841

Cardoso RM, Soares PM (2022) Is there added value in the EURO-CORDEX hindcast temperature simulations? Assessing the added value using climate distributions in Europe. Int J Climatol 42:4024–4039

Careto JAM, Soares PMM, Cardoso RM, Herrera S, Gutiérrez JM (2022) Added value of EURO-CORDEX high-resolution downscaling over the Iberian Peninsula revisited-Part 2: max and min temperature. Geosci Model Dev 15(6):2653–2671

Carvalho D, Cardoso Pereira S, Rocha A (2021) Future surface temperatures over Europe according to CMIP6 climate projections: an analysis with original and bias-corrected data. Clim Change 167:1–17

Chen H, Sun J, Lin W, Xu H (2020) Comparison of CMIP6 and CMIP5 models in simulating climate extremes. Sci Bull 65(17):1415–1418

Cherchi A, Fogli PG, Lovato T, Peano D, Iovino D, Gualdi S et al (2019) Global mean climate and main patterns of variability in the CMCC-CM2 coupled model. J Adv Model Earth Syst 11(1):185–209

Choudhury D, Ji F, Nishant N, Di Virgilio G (2023) Evaluation of ERA5-simulated temperature and its extremes for Australia. Atmosphere 14(6):913

Collazo S, Barrucand M, Rusticucci M (2022) Evaluation of CMIP6 models in the representation of observed extreme temperature indices trends in South America. Clim Change 172(1):21

Consortium EE et al (2019) IPCC DDC: EC-Earth-Consortium EC-Earth3 model output prepared for CMIP6 CMIP amip

Consortium EE et al (2019) IPCC DDC: EC-Earth-Consortium EC-Earth3-Veg model output prepared for CMIP6 ScenarioMIP

Danabasoglu G, Lamarque JF, Bacmeister J, Bailey D, DuVivier A, Edwards J et al (2020) The community earth system model version 2 (CESM2). J Adv Model Earth Syst 12(2):e2019MS001916

Dias CG, Reboita MS (2021) Assessment of CMIP6 simulations over tropical South America. Revista Brasileira de Geografia Física 14(3):1282–1295

Díaz J, Sáez M, Carmona R, Mirón IJ, Barceló MA, Luna MY et al (2019) Mortality attributable to high temperatures over the 2021–2050 and 2051–2100 time horizons in Spain: adaptation and economic estimate. Environ Res 172:475–485. https://doi.org/10.1016/j.envres.2019.02.041

Donat MG, Alexander LV, Herold N, Dittus AJ (2016) Temperature and precipitation extremes in century-long gridded observations, reanalyses, and atmospheric model simulations. J Geophys Res Atmos 121(19):11–174

Dunne JP, Horowitz L, Adcroft A, Ginoux P, Held I, John J et al (2020) The GFDL Earth System Model version 4.1 (GFDL-ESM 4.1): overall coupled model description and simulation characteristics. J Adv Model Earth Syst 12(11):e2019MS002015

Eyring V, Bony S, Meehl GA, Senior CA, Stevens B, Stouffer RJ et al (2016) Overview of the Coupled Model Intercomparison Project Phase 6 (CMIP6) experimental design and organization. Geosci Model Dev 9(5):1937–1958
Fan X, Duan Q, Shen C, Wu Y, Xing C (2020) Global surface air temperatures in CMIP6: historical performance and future changes. Environ Res Lett 15(10):104056
Fischer EM, Knutti R (2015) Anthropogenic contribution to global occurrence of heavy-precipitation and high-temperature extremes. Nat Clim Chang 5(6):560–564
Fischer EM, Schär C (2009) Future changes in daily summer temperature variability: driving processes and role for temperature extremes. Clim Dyn 33(7–8):917–935
Geirinhas JL, Russo A, Libonati R, Trigo RM, Castro LC, Peres LF et al (2020) Heat-related mortality at the beginning of the twenty-first century in Rio de Janeiro, Brazil. Int J Biometeorol 64:1319–1332
Gleixner S, Demissie T, Diro GT (2020) Did ERA5 improve temperature and precipitation reanalysis over East Africa? Atmosphere 11(9):996
Goosse H, Braida M, Crosta X, Mairesse A, Masson-Delmotte V, Mathiot P et al (2012) Antarctic temperature changes during the last millennium: evaluation of simulations and reconstructions. Quatern Sci Rev 55:75–90
Grose MR, Narsey S, Delage F, Dowdy AJ, Bador M, Boschat G et al (2020) Insights from CMIP6 for Australia's future climate. Earth's Future 8(5):e2019EF001469
Gutiérrez C, Molina M, Ortega M, Lopez-Franca N, Sánchez E (2024) Low-wind climatology (1979–2018) over Europe from ERA5 reanalysis. Climate Dynamics, pp 1–16
Gutjahr O, Putrasahan D, Lohmann K, Jungclaus JH, von Storch JS, Brüggemann N et al (2019) Max planck institute earth system model (MPI-ESM1. 2) for the high-resolution model intercomparison project (HighResMIP). Geosci Model Dev 12(7):3241–3281
Hamed MM, Nashwan MS, Shahid S, bin Ismail T, Wang Xj, Dewan A et al (2022) Inconsistency in historical simulations and future projections of temperature and rainfall: a comparison of CMIP5 and CMIP6 models over Southeast Asia. Atmos Res 265:105927
Hansen J, Sato M (2016) Regional climate change and national responsibilities. Environ Res Lett 11(3):034009
Hansen J, Sato M, Ruedy R (2012) Perception of climate change. Proc Natl Acad Sci 109(37):E2415–E2423
Harrington LJ (2021) Temperature emergence at decision-relevant scales. Environ Res Lett 16(9):094018
Hersbach H, Bell B, Berrisford P, Hirahara S, Horányi A, Muñoz-Sabater J et al (2020) The ERA5 global reanalysis. Q J R Meteorol Soc 146(730):1999–2049
Hersbach H, Bell B, Berrisford P, Biavati G, Horányi A, Muñoz Sabater J et al (2018) ERA5 hourly data on single levels from 1979 to present. Copernicus climate change service (c3s) climate data store (cds) 10(10.24381)
Hersbach H, Bell W, Berrisford P, Horányi A, J MS, Nicolas J et al (2019) Global reanalysis: goodbye ERA-Interim, hello ERA5. ECMWF Newsletter, pp 17–24. https://doi.org/10.21957/vf291hehd7
Huntingford C, Jones PD, Livina VN, Lenton TM, Cox PM (2013) No increase in global temperature variability despite changing regional patterns. Nature 500(7462):327–330
Iturbide M, Gutiérrez JM, Alves LM, Bedia J, Cerezo-Mota R, Cimadevilla E et al (2020) An update of IPCC climate reference regions for subcontinental analysis of climate model data: definition and aggregated datasets. Earth Syst Sci Data 12(4):2959–2970. https://doi.org/10.5194/essd-12-2959-2020
Jain S, Scaife AA, Shepherd TG, Deser C, Dunstone N, Schmidt GA et al (2023) Importance of internal variability for climate model assessment. npj Clim Atmos Sci 6(1):68
Kim YH, Min SK, Zhang X, Sillmann J, Sandstad M (2020) Evaluation of the CMIP6 multi-model ensemble for climate extreme indices. Weather Clim Extrem 29:100269
Kreyling J (2010) Winter climate change: a critical factor for temperate vegetation performance. Ecology 91(7):1939–1948
Lee J, Kim J, Sun MA, Kim BH, Moon H, Sung HM et al (2020) Evaluation of the Korea meteorological administration advanced community earth-system model (K-ACE). Asia-Pac J Atmos Sci 56:381–395
Lehner F, Deser C, Maher N, Marotzke J, Fischer EM, Brunner L et al (2020) Partitioning climate projection uncertainty with multiple large ensembles and CMIP5/6. Earth Syst Dyn 11(2):491–508
Li L, Yu Y, Tang Y, Lin P, Xie J, Song M et al (2020) The flexible global ocean-atmosphere-land system model grid-point version 3 (FGOALS-g3): description and evaluation. J Adv Model Earth Syst 12(9):2012e2019MS00
Liu R, Zhang X, Wang W, Wang Y, Liu H, Ma M et al (2024) Global-scale ERA5 product precipitation and temperature evaluation. Ecol Ind 166:112481. https://doi.org/10.1016/j.ecolind.2024.112481
Lovino MA, Pierrestegui MJ, Müller OV, Berbery EH, Müller GV, Pasten M (2021) Evaluation of historical CMIP6 model simulations and future projections of temperature and precipitation in Paraguay. Clim Change 164:1–24
Maraun D (2016) Bias correcting climate change simulations-a critical review. Curr Clim Change Rep 2:211–220

Meehl GA, Boer GJ, Covey C, Latif M, Stouffer RJ (2000) The coupled model intercomparison project (CMIP). Bull Am Meteor Soc 81(2):313–318
Molina MO, Careto J, Gutiérrez C, Sánchez E, Goergen K, Sobolowski S et al (2024) The added value of simulated near-surface wind speed over the Alps from a km-scale multimodel ensemble. Climate Dynamics, pp 1–19
Molina M, Sánchez E, Gutiérrez C (2020) Future heat waves over the Mediterranean from an Euro-CORDEX regional climate model ensemble. Sci Rep 10(1):8801
Molina MO, Gutiérrez C, Sánchez E (2021) Comparison of ERA5 surface wind speed climatologies over Europe with observations from the HadISD dataset. Int J Climatol 41(10):4864–4878
Molina MO, Careto JAM, Gutiérrez C, Sánchez E, Soares PMM (2022) The added value of high-resolution EURO-CORDEX simulations to describe daily wind speed over Europe. Int J Climatol 43(2):1062–1078
Nie S, Fu S, Cao W, Jia X (2020) Comparison of monthly air and land surface temperature extremes simulated using CMIP5 and CMIP6 versions of the Beijing Climate Center climate model. Theoret Appl Climatol 140:487–502
Nijsse FJ, Cox PM, Huntingford C, Williamson MS (2019) Decadal global temperature variability increases strongly with climate sensitivity. Nat Clim Chang 9(8):598–601
on Climate Change (IPCC) IP (2023) In: Weather and climate extreme events in a changing climate. Cambridge University Press, pp 1513–1766
O'Neill BC, Tebaldi C, Van Vuuren DP, Eyring V, Friedlingstein P, Hurtt G et al (2016) The scenario model intercomparison project (ScenarioMIP) for CMIP6. Geosci Model Dev 9(9):3461–3482
Ortega G, Arias PA, Villegas JC, Marquet PA, Nobre P (2021) Present-day and future climate over central and South America according to CMIP5/CMIP6 models. Int J Climatol 41(15):6713–6735
Patterson M (2023) North-West Europe hottest days are warming twice as fast as mean summer days. Geophys Res Lett 50(10):e2023GL102757
Roffe SJ, van der Walt AJ (2023) Representation and evaluation of southern Africa's seasonal mean and extreme temperatures in the ERA5-based reanalysis products. Atmos Res 284:106591
Rohat G, Flacke J, Dosio A, Pedde S, Dao H, van Maarseveen M (2018) Influence of changes in socioeconomic and climatic conditions on future heat-related health challenges in Europe. Global and planetary change
Rong X (2023) IPCC DDC: CAMS CAMS_CSM1.0 model output prepared for CMIP6 CMIP. World Data Center for Climate (WDCC) at DKRZ. https://doi.org/10.26050/WDCC/AR6.C6CMCAMCC0
Rummukainen M (2012) Changes in climate and weather extremes in the 21st century. Wiley Interdiscip Rev Clim Change 3(2):115–129
Saurral RI, Raggio GA (2023) Changes in stratospheric ozone concentrations shape air temperature distributions on the Antarctic Peninsula. Theoret Appl Climatol 154(3):815–831
Schneider T, Bischoff T, Haug GH (2014) Migrations and dynamics of the intertropical convergence zone. Nature 513(7516):45–53
Schulzweida U, Kornblueh L, Quast R (2019) CDO user guide
Seland Ø, Bentsen M, Olivié D, Toniazzo T, Gjermundsen A, Graff LS et al (2020) Overview of the Norwegian Earth System Model (NorESM2) and key climate response of CMIP6 DECK, historical, and scenario simulations. Geosci Model Dev 13(12):6165–6200
Sellar AA, Jones CG, Mulcahy JP, Tang Y, Yool A, Wiltshire A et al (2019) UKESM1: description and evaluation of the UK Earth System Model. J Adv Model Earth Syst 11(12):4513–4558
Semmler T, Danilov S, Gierz P, Goessling HF, Hegewald J, Hinrichs C et al (2020) Simulations for CMIP6 with the AWI climate model AWI-CM-1-1. J Adv Model Earth Syst 12(9):e2019MS002009
Seneviratne SI, Nicholls N, Easterling D, Goodess CM, Kanae S, Kossin J et al (2012) In: Changes in climate extremes and their impacts on the natural physical environment. Cambridge University Press, pp 109–230
Seneviratne SI, Hauser M (2020) Regional climate sensitivity of climate extremes in CMIP6 versus CMIP5 multimodel ensembles. Earth's future 8(9):e2019EF001474
Simmons A, Berrisford P, Dee D, Hersbach H, Hirahara S, Thépaut JN (2017) A reassessment of temperature variations and trends from global reanalyses and monthly surface climatological datasets. Q J R Meteorol Soc 143(702):101–119
Soares PM, Cardoso RM, Miranda PM, de Medeiros J, Belo-Pereira M, Espirito-Santo F (2012) WRF high resolution dynamical downscaling of ERA-Interim for Portugal. Clim Dyn 39:2497–2522
Sobie S, Zwiers F, Curry C (2021) Climate model projections for Canada: a comparison of CMIP5 and CMIP6. Atmos Ocean 59(4–5):269–284
Soci C, Hersbach H, Simmons A, Poli P, Bell B, Berrisford P et al (2024) The ERA5 global reanalysis from 1940 to 2022. Q J R Meteorol Soc 150(764):4014–4048
Suarez-Gutierrez L, Müller WA, Li C, Marotzke J (2020) Dynamical and thermodynamical drivers of variability in European summer heat extremes. Clim Dyn 54:4351–4366

Swart NC, Cole JN, Kharin VV, Lazare M, Scinocca JF, Gillett NP et al (2019) The Canadian earth system model version 5 (CanESM5. 0.3). Geosci Model Dev 12(11):4823–4873
Tatebe H, Ogura T, Nitta T, Komuro Y, Ogochi K, Takemura T et al (2019) Description and basic evaluation of simulated mean state, internal variability, and climate sensitivity in MIROC6. Geosci Model Dev 12(7):2727–2765
Taylor KE (2024) Truly conserving with conservative remapping methods. Geosci Model Dev 17(1):415–430. https://doi.org/10.5194/gmd-17-415-2024
Tebaldi C, Debeire K, Eyring V, Fischer E, Fyfe J, Friedlingstein P et al (2021) Climate model projections from the Scenario Model Intercomparison Project (ScenarioMIP) of CMIP6. Earth Syst Dyn 12(1):253–293. https://doi.org/10.5194/esd-12-253-2021
Tian D, Guo Y, Dong W (2015) Future changes and uncertainties in temperature and precipitation over China based on CMIP5 models. Adv Atmos Sci 32:487–496
Turner J, Marshall GJ, Clem K, Colwell S, Phillips T, Lu H (2020) Antarctic temperature variability and change from station data. Int J Climatol 40(6):2986–3007
Turner J, Lu H, King J, Marshall GJ, Phillips T, Bannister D et al (2021) Extreme temperatures in the Antarctic. J Clim 34(7):2653–2668
Vautard R, Cattiaux J, Happé T, Singh J, Bonnet R, Cassou C et al (2023) Heat extremes in Western Europe are increasing faster than simulated due to missed atmospheric circulation changes
Velikou K, Lazoglou G, Tolika K, Anagnostopoulou C (2022) Reliability of the ERA5 in replicating mean and extreme temperatures across Europe. Water 14(4):543
Voldoire A, Saint-Martin D, Sénési S, Decharme B, Alias A, Chevallier M et al (2019) Evaluation of CMIP6 deck experiments with CNRM-CM6-1. J Adv Model Earth Syst 11(7):2177–2213
Volodin EM, Mortikov EV, Kostrykin SV, Galin VY, Lykossov VN, Gritsun AS et al (2018) Simulation of the modern climate using the INM-CM48 climate model. Russ J Numer Anal Math Model 33(6):367–374
Wang C, Graham RM, Wang K, Gerland S, Granskog MA (2019) Comparison of ERA5 and ERA-Interim near-surface air temperature, snowfall and precipitation over Arctic sea ice: effects on sea ice thermodynamics and evolution. Cryosphere 13(6):1661–1679
Wang YC, Hsu HH, Chen CA, Tseng WL, Hsu PC, Lin CW et al (2021) Performance of the Taiwan earth system model in simulating climate variability compared with observations and CMIP6 model simulations. J Adv Model Earth Syst 13(7):e2020MS002353
Wu T, Yu R, Lu Y, Jie W, Fang Y, Zhang J et al (2021) BCC-CSM2-HR: a high-resolution version of the Beijing Climate Center Climate System Model. Geosci Model Dev 14(5):2977–3006
Xian T, Xia J, Wei W, Zhang Z, Wang R, Wang LP et al (2021) Is Hadley cell expanding? Atmosphere 12(12):1699
Yilmaz M (2023) Accuracy assessment of temperature trends from ERA5 and ERA5-Land. Sci Total Environ 856:159182
Yukimoto S, Kawai H, Koshiro T, Oshima N, Yoshida K, Urakawa S et al (2019) The Meteorological Research Institute Earth System Model version 2.0, MRI-ESM2. 0: description and basic evaluation of the physical component. J Meteorol Soc Jpn Ser II 97(5):931–965
Zelinka MD, Myers TA, McCoy DT, Po-Chedley S, Caldwell PM, Ceppi P et al (2020) Causes of higher climate sensitivity in CMIP6 models. Geophys Res Lett 47(1):e2019GL085782
Zhongming Z, Linong L, Xiaona Y, Wangqiang Z, Wei L et al (2022) AR6 synthesis report: climate change 2022
Zhu J, Xie A, Qin X, Wang Y, Xu B, Wang Y (2021) An assessment of ERA5 reanalysis for antarctic near-surface air temperature. Atmosphere 12(2). https://doi.org/10.3390/atmos12020217
Ziehn T, Chamberlain MA, Law RM, Lenton A, Bodman RW, Dix M et al (2020) The Australian earth system model: ACCESS-ESM1. 5. J South Hemisph Earth Syst Sci 70(1):193–214